Separation and Purification Technology 299 (2022) 121693

Contents lists available at ScienceDirect

Separation and Purification Technology

journal homepage: www.elsevier.com/locate/seppur

Thin film nanocomposite membranes of PIM-1 and graphene oxide/ZIF-8 nanohybrids for organophilic pervaporation

Boya Qiu [a], Monica Alberto [a], Sajjad Mohsenpour [a], Andrew B. Foster [b], Shengzhe Ding [a], Zunmin Guo [a], Shaojun Xu [a], Stuart M. Holmes [a], Peter M. Budd [b], Xiaolei Fan [a], Patricia Gorgojo [a,c,d,*]

[a] Department of Chemical Engineering, Faculty of Science and Engineering, The University of Manchester, Manchester M13 9PL, United Kingdom
[b] Department of Chemistry, Faculty of Science and Engineering, The University of Manchester, Manchester M13 9PL, United Kingdom
[c] Instituto de Nanociencia y Materiales de Aragón (INMA) CSIC-Universidad de Zaragoza, C/ Mariano Esquillor s/n, 50018 Zaragoza, Spain
[d] Departamento de Ingeniería Química y Tecnologías del Medio Ambiente, Universidad de Zaragoza, C/ Pedro Cerbuna 12, 50009 Zaragoza, Spain

ARTICLE INFO

Keywords:
Graphene oxide (GO)
pervaporation (PV)
PIM-1
Thin-film nanocomposite (TFN) membrane
ZIF-8/GO

ABSTRACT

In this work, thin film nanocomposite (TFN) membranes of super-glassy polymer PIM-1 containing zeolitic imidazolate framework-8 (ZIF-8)/graphene oxide (GO) composites (ZG) have been prepared by dip-coating onto water pre-impregnated polyvinylidene fluoride (PVDF) substrates. Higher flux and improved separation factors as compared to bare PIM-1 thin film composite (TFC) membranes have been achieved in organophilic pervaporation; for an aqueous feed solution with 5 wt% of butanol at 65 °C, a total permeate flux of 7.9 ± 0.69 kg $m^{-2}h^{-1}$ and a separation factor ($\beta_{BtOH/H2O}$) of 29.9 ± 1.99 have been obtained with a TFC membrane containing 0.5 wt% of ZG filler. The pervaporation separation index (PSI) of this membrane (228 kg $m^{-2}h^{-1}$) is amongst the highest values reported in the literature. This excellent performance is attributed to the formation of a defect-free PIM-1 active layer (<1 μm) and the hydrophobic nature of the ZG fillers.

1. Introduction

Pervaporation (PV) is a membrane-based technology that can potentially replace some energy-intensive distillation processes currently used for industrial separations [1]. For instance, organophilic PV can be used for the recovery of bio-organics (such as acetone, butanol, and ethanol) from fermentation broths, avoiding this way product inhibition and increasing product yield [2–4]. Currently, polydimethylsiloxane (PDMS), poly[1-(trimethylsilyl)-1-propyne] (PTMSP), polyether block amide (PEBA), and polymers of intrinsic microporosity (PIMs) membranes, are used for the preparation of PV membranes for bio-alcohol recovery at laboratory scale [5–9]. Among PIMs, PIM-1, with a unique rigid and contorted ladder-like backbone and soluble in only a few solvents, show outstanding permeability and fair separation factors compared to conventional rubbery polymer membranes [5,10,11].

Freestanding films of PIM-1, several tens of micron thick, are typically prepared at laboratory scale for PV applications and they are ideal for lab-scale investigation. However, thin-film composite (TFC) membranes are the preferred configuration for large-scale PV processes due to their higher flux (typically the flux is inversely proportional to the membrane thickness) and good mechanical stability [12,13]. One issue when working with TFCs is the infiltration of the polymer solution in the pores of the substrate during the coating process, which creates additional mass transfer resistance and can lead to defects in the thin separation layer [10,14]. To date, the highest reported flux of a PIM-1 TFC membrane prepared onto conventional asymmetric polymer substrates for the PV of *n*-butanol/water mixtures is 9 kg $m^{-2}h^{-1}$, with a separation factor of 13.3 [11]. The control of the pore size and surface porosity of the support allowed for the formation of a TFC with a PIM-1 layer of just 1 μm in thickness. The bigger the pore size of the substrate, the higher the polymer infiltration. It is generally accepted that a little penetration of the active layer into the substrate imparts mechanical stability to a TFC membrane. However, it is difficult to assess how much is the optimum degree of penetration, or if it is possible to completely prevent it without affecting stability and reducing as much as possible mass transfer resistance. If substrates with higher porosity are to be used to further decrease their contribution to mass transfer resistance, for instance electrospun supports such as those recently published by our

* Corresponding author at: Departmento de Ingeniería Química y Tecnologías del Medio Ambiente, Universidad de Zaragoza, Spain.
E-mail addresses: pgorgojo@unizar.es, p.gorgojo@unizar.es (P. Gorgojo).

https://doi.org/10.1016/j.seppur.2022.121693
Received 3 June 2022; Received in revised form 6 July 2022; Accepted 7 July 2022
Available online 12 July 2022

Nomenclature

m_i	Mass of components
J	Membrane flux
m	Mass of permeate collected
A	Membrane of area
α	Selectivity
X	Mole fractions of the component in feed side
Y	Mole fractions of the component in the permeate side
PSI	Pervaporation separation index
$J_{o,i}$	Pre-exponential factors
$E_{J,i}$	Apparent activation energies of the flux of component i
R	Ideal gas constant
T	Feed temperature
E_a	Apparent activation energy
P_i	The permeability of component i
β	Separation factor
p_i	The partial pressure of component i
γ_i	Activity coefficient and mole fraction of component i
χ_i	Mole fraction of component i
p_i^{sat}	Saturation vapour pressure of the pure component i

research group [15], one strategy to avoiding PIM-1 infiltration is by filling the pores of the substrate with a solvent prior to dip/kiss coating; our research group reported the use of a range of solvents (ethanol, methanol and chloroform) to pre-fill the pores of these highly porous PVDF electrospun substrates for the preparation of high-flux PIM-1 TFCs. Yet, the prepared TFCs showed low separation factors of ~8 due to defects/pinholes that were formed by the rapid interdiffusion between the two miscible liquids (the impregnating solvent and chloroform from the coating solution) during the formation of the PIM-1 layer. Herein, the use of immiscible solvent systems (water/chloroform) for a more stable interface is proposed.

In addition to increased flux, the ability to perform more effective separations (i.e. higher separation factors) is equally important. In an attempt to favour the permeation of organic compounds over water, a variety of micro- or nanofiller materials (e.g., zeolites, carbon nanotubes (CNTs), graphene oxide (GO), metal–organic frameworks (MOFs), and covalent organic frameworks (COFs)) have been successfully incorporated into free-standing polymeric PV membranes [16–20]. Among them, MOFs such as ZIF-8 [21,22], ZIF-71 [23,24], MIL-53 [25], with versatile/tuneable pore structures and functionalities as well as good compatibility with polymers, show promising for organophilic separations. Specifically, ZIF-8 nanoparticles with inner superhydrophobicity channels accompanied by a 'gate-opening' effect, can create preferential pathways for the permeation of organic compound, and have been reported to improve the organic/water separation performance of rubbery polymer membranes [26]. However, it is still challenging to prepare defect-free PIM-1 TFN membranes, where suitable fillers must be in the nanometre range due to the low thickness of their active layers. Some work on PIM-1-based TFNs for gas separation has been reported [27,28], but little data is available on PIM-1 TFNs for pervaporation. Nanosized MOFs tend to aggregate to minimize their surface energies, and thus additional non-selectivity voids can be created when they are added into a thin polymer layer. In an attempt to avoid aggregation, nanosized ZIF-8 was grown on GO and used as fillers in polydimethylsiloxane (PDMS) [29] and polyether block amide (PEBA) [30] membranes. The use of the 2D ZIF-8/GO fillers can simultaneously provide additional mass transfer pathways with high organophilic selectivity and help to reduce the active layer infiltration by partial blockage of the substrate pores during the coating process.

In this work, we investigate, for the first time, the incorporation of ZIF-8/GO nanohybrids into thin films of PIM-1 to obtain TFNs with defect-free active layers and PIM-1-infiltration-free substrates for improved flux and separation of alcohols. The PV performance of the membranes for butanol/water mixtures is systematically investigated, by varying the ZIF-8 synthesis time on GO, filler loading, and thickness of the active layers. Moreover, PIM-1 TFN membranes with different fillers including ZIF-8/GO, ZIF-8, and GO are compared to evaluate potential synergistic effects between ZIF-8 and GO in the TFN membranes.

2. Methods

2.1. Materials and chemicals

GO was purchased from William Blythe Ltd (United Kingdom). Monomers of PIM-1 (including 2,3,5,6,-tetrafluoroterephthalonitrile (TFTPN) and 5,5′,6,6′-tetrahydroxy-3,3,3′,3′-tetramethyl-1,1′-spirobisindane (TTSBI)) were acquired from Fluorochem Ltd and Alfa Aesar (UK), respectively. TFTPN was used as supplied, whilst TTSBI required further purification. The purification of TTSBI was carried out as follows: TTSBI (40 g) was placed in a 3 L round bottom flask. The flask was fitted with a 3-neck connector holding a reflux condenser and N_2 inlet. After adding ethyl acetate (667 mL) into the flask, the mixture was refluxed (90 °C) until the dissolution of TTSBI neared its completion. Then, hexane (667 mL) was added (still under reflux), and the mixture was stirred for 10 min, cooled down to room temperature and then chilled in an ice bath for 3 h. The product was filtered using a sintered funnel, and then dried in a vacuum desiccator for 24 h before use. All the other chemicals were used as received.

Polyvinylidene fluoride (PVDF, $M_w \sim 5.34 \times 10^5$ g mol^{-1}) was purchased from Sigma-Aldrich. Polypropylene/polyethylene non-woven fabric was purchased from Freudenberg Filtration Tech Ltd (Germany). Methanol (MeOH), 1-butanol (BtOH), ethanol (EtOH), acetone, dimethylacetamide (DMAc), n,n-dimethylformamide (DMF), chloroform, phosphoric acid (37 wt% in water), zinc nitrate hexahydrate ($Zn(NO_3)_2{\cdot}6H_2O$, 99%), 2-methylimidazole (2-mIm, 98%) were supplied by Sigma-Aldrich. All reagents were used without further purification.

2.2. Preparation of fillers

ZIF-8/GO nanohybrids (ZG) were prepared following the method reported by Hu et al. [31] with slight modifications. The procedure is as illustrated in Fig. 1(A). In detail, 3.2 mL GO aqueous solution was diluted with 12.8 mL MeOH. After sonication for 2 h, the GO solution was mixed with 24 mL of 2-mIm solution (1.622 g). 40 mL of $Zn(NO_3)_2{\cdot}6H_2O$ (0.732 g) was added under vigorous stirring and the mixture was then kept stirring for varying reaction times (10–80 min) at room temperature to obtain different loading of ZIF-8 on GO. The solid products were separated by centrifugation (at 10,000 rpm for 10 min), washed with DMF three times, and then washed with chloroform three times. Finally, the resulting material was dispersed in chloroform before use. The nanocomposites were named as ZG_n, where n represents the synthesis time (in min).

To prepare non-supported ZIF-8, that is bulk ZIF-8, 40 mL of $Zn(NO_3)_2{\cdot}6H_2O$ (0.732 g) was added to a 40 mL 2-mIm solution (1.622 g) under vigorous stirring. The mixture was stirred at room temperature for 80 min. The solid products were separated by centrifugation (10,000 rpm for 10 min), washed with DMF three times, and then washed with chloroform three times. Finally, the ZIF-8 was dispersed in chloroform before use.

2.3. Preparation of water impregnated PVDF substrates and PIM-1 TFN membranes

Porous PVDF support membranes were prepared following a phase inversion procedure reported elsewhere [11]. Water cannot directly penetrate the pores of the PVDF substrate due to its hydrophobic nature.

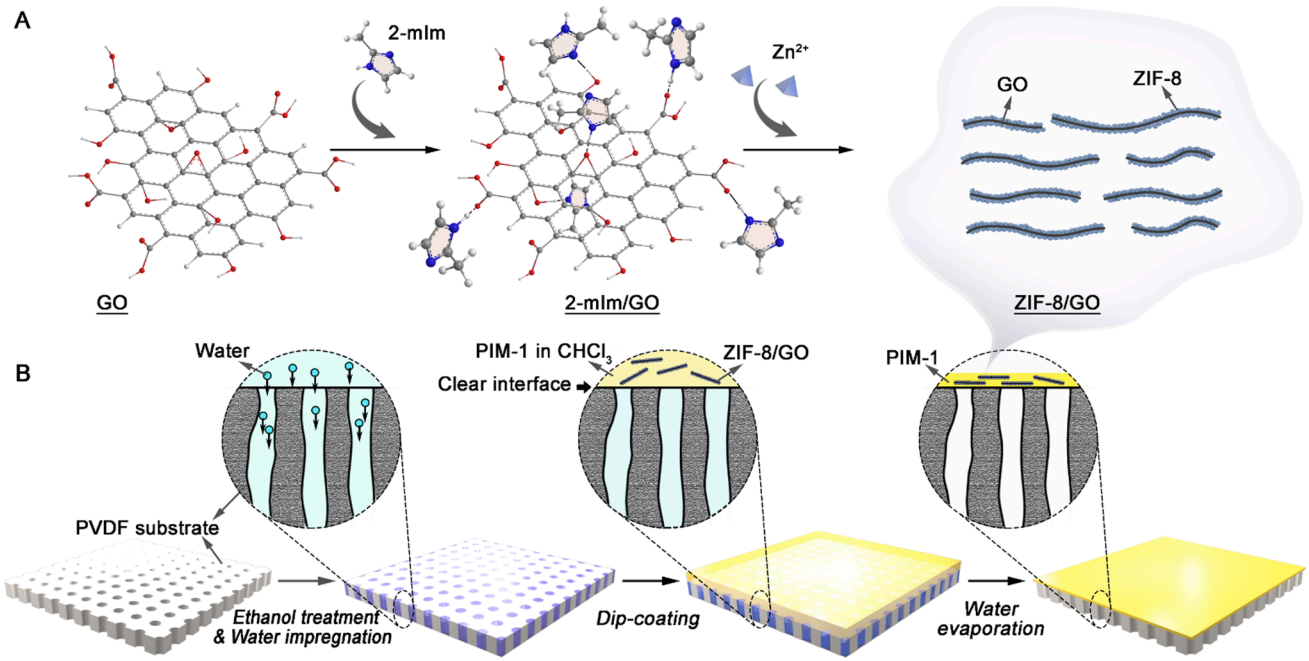

Fig. 1. Schematic of the PIM-1 TFN membranes preparation (A: preparation of ZIF-8/GO nanohybrids, ZG; B: preparation of the TFN membranes by dip-coating of water-impregnated PVDF substrate with ZG/PIM-1 solutions).

Therefore, as illustrated in Fig. 1(B), it was first immersed in ethanol for 20 min, and then placed into deionized (DI) water for 1 h to exchange the ethanol inside the pores with water. Prior to the dip-coating of PIM-1 solutions, the excess water on the surface of the PVDF was wiped out using tissue paper.

PIM-1 was synthesized as described in the Supporting Information (SI) following a modified reported procedure [5,32]. Polymeric solutions with different PIM-1 concentrations (1–5 wt%) and different loadings of ZG (0.25–1.00 wt%) were used to prepare TFN membranes via dip-coating. The filler loading (ψ) in the composite membrane (in percentage) is defined by Eq. (1).

$$\psi = \frac{m_{\text{filler}}}{m_{\text{filler}} + m_{\text{PIM - 1}}} \times 100\% \quad (1)$$

where m_{filler} is the weight of filler, and $m_{\text{PIM-1}}$ is the weight of the polymer in the membrane.

The dip-coating procedure for the preparation of TFCs and TFNs is described in the SI. Membranes were tested fresh (i.e. one day after preparation) for PV without any further treatment. The nanocomposite membranes were named $ZG_{n/x}$/PIM-1_y TFN, where x and y represent the filler loading (wt%) and the concentration of PIM-1 (wt%), respectively. When $y = 2.0$ (for most of the prepared membranes) the value is omitted in the notation. PIM-1-based TFNs containing free-standing ZIF-8 (ZIF-8_x/PIM-1 TFN) and pristine GO (GO_x/PIM-1 TFN) were also prepared using the same procedure for comparison.

2.4. Fillers and membranes characterization

The fillers and membranes were characterized using X-ray powder diffraction (XRD), attenuated total reflectance Fourier transform infrared spectroscopy (ATR-FTIR), X-ray photoelectron spectroscopy (XPS), atomic force microscopy (AFM), N_2 adsorption/desorption, thermogravimetric analysis (TGA), scanning transmission electron microscopy (STEM), water contact angles, solvent uptake, and swelling degree. More detail can be found in the SI.

2.5. Pervaporation

For the PV of alcohol/water mixtures, an aqueous solution with a concentration range of 1–5 wt% of organics was kept at a constant temperature between 35 and 75 °C using a water bath. Vacuum at 0.2 mbar was applied and kept constant on the permeate side of the membrane, and the permeate vapour was cooled by liquid nitrogen and collected in a trap. At least 1 h was required to reach steady state, and the testing was carried out for 2 h. More details on the PV testing procedure can be found in a previous publication [11]. The total flux, J (kg $m^{-2}h^{-1}$), was calculated using Eq. (5):

$$J = \frac{m}{A \cdot t} \quad (5)$$

where m (kg) is the mass of permeate collected over time t (h) for a given membrane area A (m^2) For each type of membrane, measurements were repeated with five membrane coupons to obtain the average value and standard deviation. Tukey significance tests have been carried out for the membrane performance and characterization data. Unless specified otherwise, statistically significant differences exist between reported results.

The concentration of the collected permeate was determined by gas chromatography (GC). Before the analysis, the collected permeated was diluted with acetone to form a homogeneous mixture. Analysis was performed using an Agilent 7820A GC system with the PoraPLOT Q-HT column (10 m × 0.32 mm × 20 μm) and flame ionization detector (FID). The procedure is described in more detail in the SI.

Separation factors were calculated using Eq. (6):

$$\beta_{i/\text{H2O}} = \frac{Y_i/(1 - Y_i)}{X_i/(1 - X_i)} \quad (6)$$

where Y_i and X_i (dimensionless) are the mole fractions of component i in the permeate and feed sides, respectively.

The overall PV membrane performance was evaluated through the PV separation index (PSI, kg $m^{-2}h^{-1}$) calculated using Eq. (7).

$$\text{PSI} = (\beta - 1) \cdot J \quad (7)$$

The relationship between the flux or permeability and feed

temperature can be determined using an Arrhenius-type equation (Eq. (8)):

$$J_i = J_{o,i}\exp\left(-\frac{E_{J,i}}{RT}\right) \tag{8}$$

$$J_i = J \cdot x_i \tag{9}$$

where J_i (kg m^{-2}h^{-1}) is the flux of component i and x_i (dimensionless) is the mass fraction of component i in the permeate, $J_{o,i}$ (kg m^{-2}h^{-1}) is the pre-exponential factor of component i, $E_{J,i}$ (kJ mol^{-1}) is the apparent activation energy of flux of component i, R is the gas constant (8.314 J mol^{-1} K^{-1}), and T is the feed temperature (K).

Normalization of the permeation flux using the driving forces is essential to interpret the intrinsic membrane properties. The permeability of component i (g m h^{-1} kPa^{-1}) and the selectivity (α, dimensionless) are calculated as follows:

$$P_i = \frac{J_i \times \delta}{\Delta p_i} \tag{10}$$

$$\Delta p_i = p_{i,f} - p_{i,p} \tag{11}$$

$$p_{i,f} = \gamma_{i,f}\chi_{i,f}p_{i,f}^{sat} \tag{12}$$

$$\alpha = \frac{P_B}{P_W} \tag{13}$$

where δ is the thickness of the active layer (m); Δp_i (kPa) is the driving force of component i across the membrane, and $p_{i,f}$ and $p_{i,p}$ (kPa) are the partial pressure of component i in the feed and permeate side, respectively. $p_{i,f}$ is calculated using Eq. (12) and the results at different butanol concentrations in the feed are shown in Table S1, and $p_{i,p}$ is assumed to be zero due to the vacuum in the permeate side; $\gamma_{i,f}$ (dimensionless) is the activity coefficient determined by the software Aspen Plus with Wilson model and are also displayed in Table S1. $\chi_{i,f}$ (dimensionless) is the mole fraction of component i in the feed side. $p_{i,f}^{sat}$ (kPa) is the saturation vapor pressure of the pure component i calculated by the Antoine equation, which is 10465.5 Pa and 25029.8 Pa for butanol and water, respectively, at 65 °C.

3. Results and discussion

3.1. Characterization of the fillers

The physicochemical properties of the ZIF-8/GO nanohybrids, ZG, were determined by XRD, FTIR, XPS, TGA and N_2 adsorption/desorption measurements (Fig. S2).

The key to forming a defect-free TFN membrane is to produce GZ where ZIF-8 is immobilized and formed as a continuous, uniform, and thin layer on top of the GO. The morphology of ZG_{80} was evaluated by TEM, SEM and AFM, as shown in Fig. 2. After ZIF-8 growth on GO, the 2D morphology of ZG (Fig. 2(A – B)) is similar to that of pristine GO (Fig. S4). The well-defined ring-shaped diffraction pattern in the inset of Fig. 2(A2) confirms the crystallinity of the supported ZIF-8 [33,34]. TEM-EDX mapping of C, O and Zn elements (Fig. 2(C)) shows the even distribution of ZIF-8 nanocrystals onto the GO flakes, which was also confirmed by SEM-EDX Mapping (Fig. S5). The thickness of pristine GO and ZG is measured by AFM, which is ~ 3 nm (Fig. 2(D1 – 2) and ~ 45 nm (Fig. 2(D3 – 4)), respectively. The average lateral flake size of ZG is about 3.9 μm (Fig. S6), that is, the aspect ratio of ZG exceeds 86. The roughness of ZG was determined by AFM at about 2.5 nm, which is much lower than the size of the bulk ZIF-8. This proved that the ZIF-8 crystals are continuously supported on GO. In ZG, ZIF-8 crystals were grown on both sides of the GO flakes, and hence the thickness of the supported ZIF-8 crystals layer was estimated at 20–30 nm.

Smaller crystal sizes of the ZIF-8 nanoparticles in the ZG are preferable to reduce the thickness of the ZG nanohybrid; besides, smaller particle sizes with higher external surface areas can lead to a bigger fraction of the polymer at the interface, thereby minimizing the number of non-selective pathways and enhance the interaction between fillers and PIM-1 chains [35,36]. The grain boundary between the supported

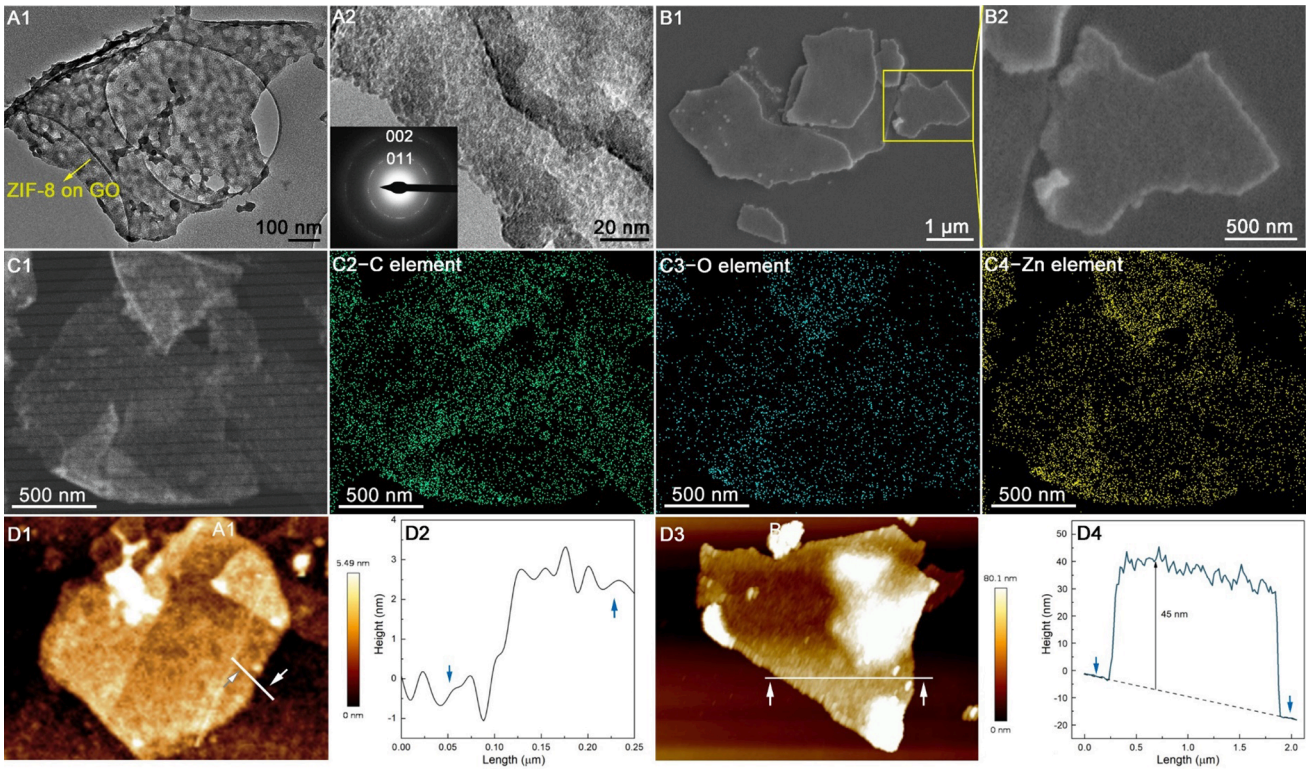

Fig. 2. HRTEM (A1 – A2), SEM (B1 – B2), TEM-EDX mapping (C1 – C4) of $ZG_{80\text{-}0.5}$, and AFM images and height profiles of GO (D1 – D2) and ZG (D3 – D4).

ZIF-8 crystals could be identified on the phase graph in the AFM of ZG_{80}, which leads to the extraction of the particle size and size distribution of the supported ZIF-8 (The calculation method of the crystal size is presented in the SI). The size of the ZIF-8 crystals is ~ 32 nm (Fig. 3(A)), which agrees well with the aforementioned estimated thickness by AFM. The size of the supported ZIF-8 is significantly smaller than that of the bulk ZIF-8 (~94 nm based on SEM analysis, Fig. 3(B)). This could be attributed to the large surface area of GO which can serve as the platform for the nucleation of ZIF-8. Besides, the large number of carboxyl groups on GO can form hydrogen bonding with − NH in 2-mIm and also form complexation with Zn^{2+}, and thus act as the nucleation sites to promote ZIF-8 synthesis [29]. Because of the well-known trade-off between nucleation sites and crystal growth, the size of the supported ZIF-8 was reduced significantly compared to that of bulk ZIF-8 crystals [29,37].

3.2. Characterization of ZG/PIM-1 TFN membranes

ZG/PIM-1 TFN membranes were prepared by dip-coating on water-impregnated PVDF substrate (the surface of pristine PVDF was characterized by SEM as shown in Fig. S7(A) and the average pore size of PVDF substrate is 61 nm (Fig. S7(B)). ZG nanohybrids were incorporated into the PIM-1 active layer of TFN membranes. XRD and XPS analyses (Fig. 4) confirm the successful incorporation; XRD patterns in Fig. 4(A) show the presence of crystalline peaks of ZG in the amorphous PIM-1 matrix, and Zn LMM peaks were detected in the XPS survey spectra of the $ZG_{80\text{-}0.5}$/PIM-1 TFN (Fig. 4(B)). ZG dispersed well in the TFN membranes evidenced by SEM-EDX analysis (Fig. S8).

To reduce mass transfer resistance, TFN membranes with thin active layers are needed to reduce the diffusion path of adsorbed species. The infiltration of the active layer in the substrate pores by dip-coating can result in a less uniform active layer with additional mass transfer resistance and should be avoided. This can be achieved by impregnating the PVDF substrates with water before dip-coating as shown in Fig. 5(A). Since water and chloroform (solvent for PIM-1) are immiscible, a stable interface between water and chloroform during the dip-coating is obtained, which prevents ZG/PIM-1 (in chloroform) from permeating into the pores of the PVDF substrate. In addition, water can be evaporated once the TFN membrane is formed, avoiding any contamination of the permeate during PV. The cross-section of the ZG/PIM-1 TFN membrane prepared by dip-coating with water-impregnation method was characterized by SEM. Thin layers of ZG/PIM-1 were formed on the PVDF substrate without defects; a clear interface can be seen between the PIM-1 active layer and PVDF substrate in the SEM picture in Fig. 5(B1). The minimum active layer thickness is 0.67 μm for the $ZG_{80\text{-}0.5}$/$PIM\text{-}1_{1.0}$ TFN membranes, with thickness increasing as a function of the concentration of PIM-1 in the coating solution, as shown in Fig. 5(B2) (the thickness was estimated from the cross-sectional images of TFNs made with PIM-1 concentrations of 1.0–5.0 wt% in the coating solution, Fig. S9). The relationship is not linear due to the increased viscosity of the PIM-1 in the chloroform solution as the concentration of PIM-1 increases. Besides, the $ZG_{80\text{-}0.5}$/$PIM\text{-}1_{1.0}$ TFN membranes show good mechanical stability, and the active layer cannot be peeled off. The effect of water-impregnation on preventing PIM-1 infiltration was also evidenced by SEM. Fig. 5(C) shows penetration of PIM-1 in a cross-sectional image of a TFN produced from a non-impregnated support, which was confirmed by visual inspection (Fig. S10) and SEM of the back side of the prepared membranes (Fig. 5D). It was found that the yellow PIM-1 was visible on

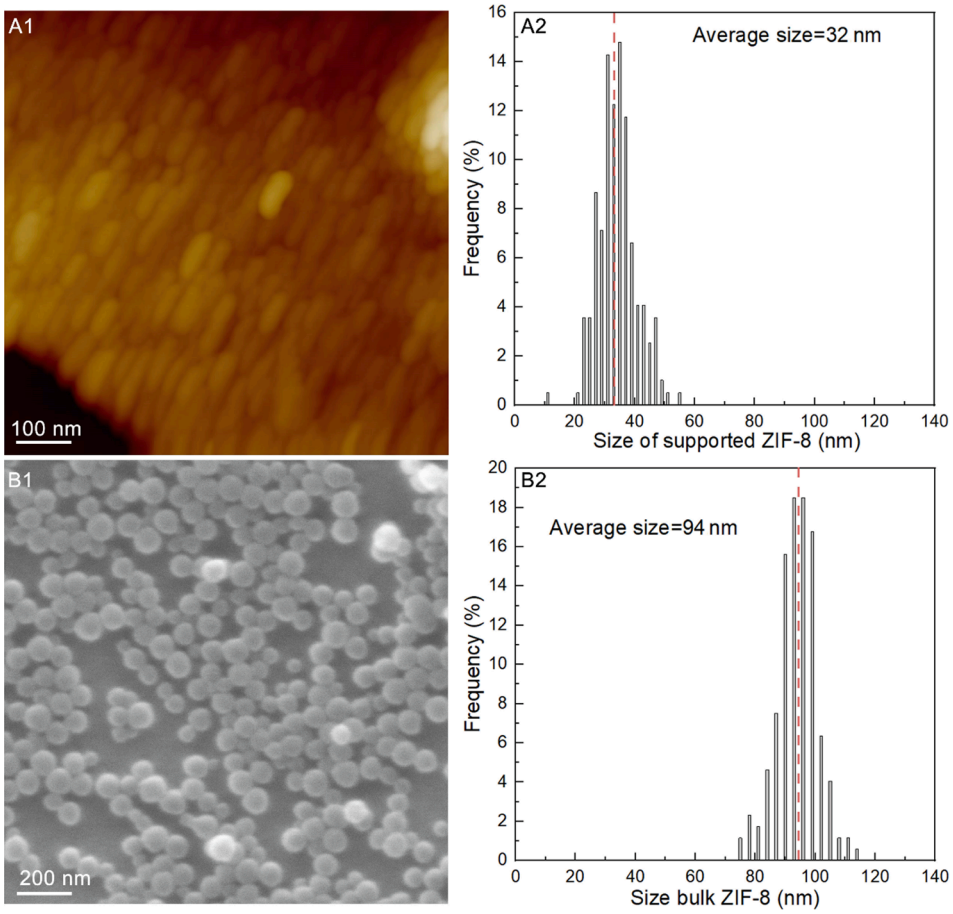

Fig. 3. Comparison of size of supported ZIF-8 and bulk ZIF-8 (A1: AFM of ZG, A2: size distribution of supported ZIF-8; B1: SEM of bulk ZIF-8; B2: size distribution of bulk ZIF-8).

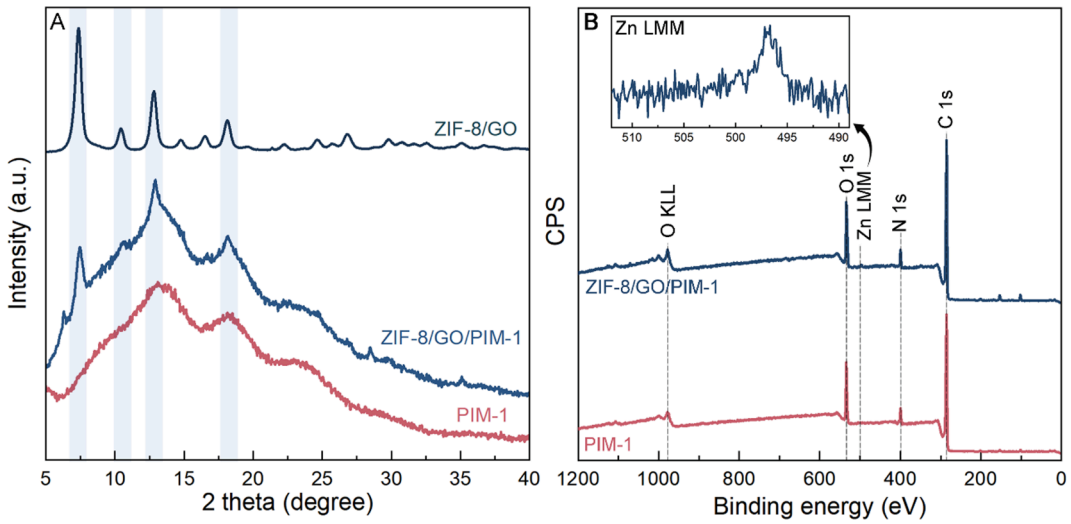

Fig. 4. XRD (A) and XPS survey spectra (B) of PIM-1 TFC membranes and $ZG_{80\text{-}0.5}$/PIM-1 TFN membranes; the inset in B is the high-resolution spectra of Zn LMM in ZG $ZG_{80\text{-}0.5}$/PIM-1 TFN membranes.

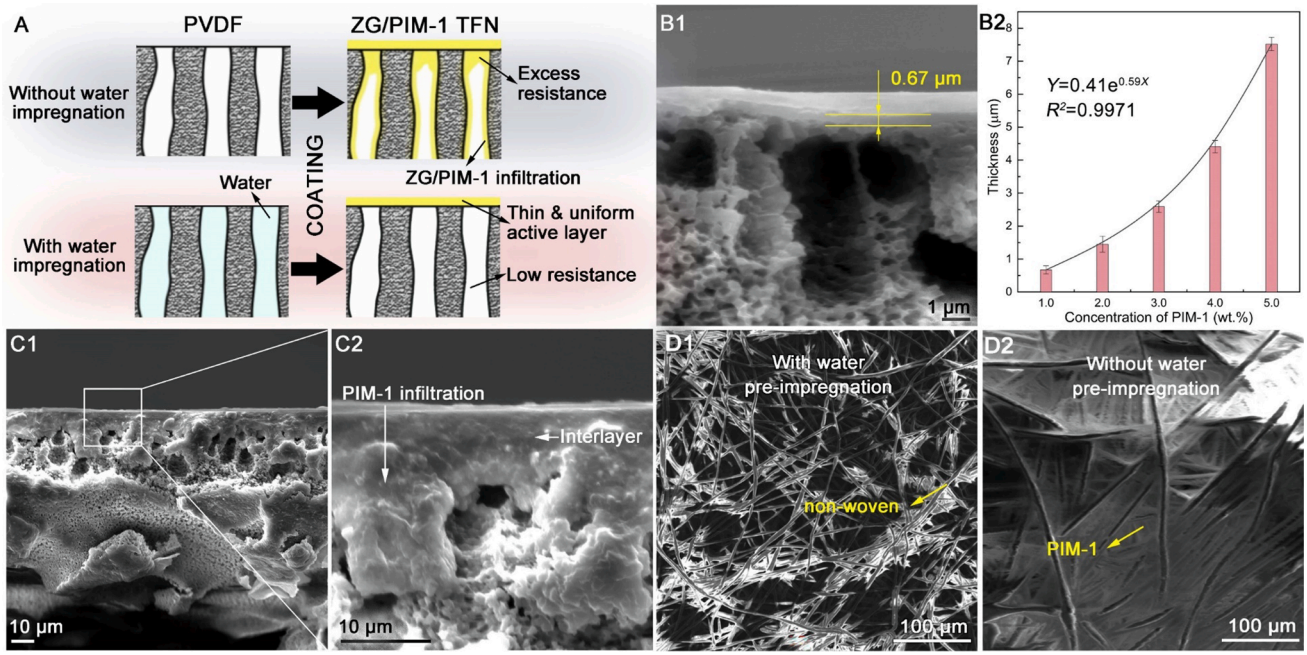

Fig. 5. Schematic of the difference between dip-coating on water-impregnated PVDF and pristine PVDF (using ZG/PIM-1 solution) (A), and cross-sectional and back side images of the ZG/PIM-1 TFN membranes. B1: cross-section of the $ZG_{80\text{-}0.5}$/$PIM\text{-}1_{1.0}$ TFN membrane prepared by dip-coating with water impregnation; B2: membrane thickness as a function of the PIM-1 concentration in the coating solution (5 membranes were measured to obtain the average value and standard deviation), the adjusted function between thickness and concentration of PIM-1 is shown as an inset; C1 – C2: cross-section of the $ZG_{80\text{-}0.5}$/$PIM\text{-}1_{2.0}$ TFN membrane coated by dip-coating without water impregnation, D1 – D2: back side of the $ZG_{80\text{-}0.5}$/$PIM\text{-}1_{2.0}$ TFN membrane prepared by dip-coating of PVDF with and without water impregnation).

the back of the PVDF after dip coating on the pristine PVDF substrate, whilst the back of the water impregnated substrate remained white (its original colour) after PIM-1 coating.

Moreover, ZG, with an average flake size of 3.9 μm, can also partially block the pore of the substrate and contribute to preventing the infiltration of the polymer. However, due to the limitation of the SEM resolution, this can only be assessed based on PV results as will be explained in Section 3.4.

The incorporation of ZG also affected the physicochemical properties of the membranes including solvent uptake, membrane swelling and water contact angle. Higher hydrophobicity was obtained as confirmed by the increase in the water contact angle, i.e., from 87.6 ± 0.97° for PIM-1 to 89.1 ± 0.68° for $ZG_{80\text{-}0.50}$/PIM-1 (Fig. 6(A)). However, both $ZIF\text{-}8_{0.50}$/PIM-1 and $GO_{0.50}$/PIM-1 had lower water contact angle that could be due to the aggregation of ZIF-8 and the hydrophilic nature of GO, respectively. $ZG_{80\text{-}0.50}$/PIM-1 membranes also showed higher solvent uptake of acetone, butanol, and ethanol than pure PIM-1 membranes (increased by 89.1, 39.5, and 39.4%, respectively) (Fig. 6(B)). The solvent uptake of $ZIF\text{-}8_{0.50}$/PIM-1 was also higher than that of neat PIM-1 TFCs and approximately equal to that of $ZG_{80\text{-}0.50}$/PIM-1. This is indeed an indication of the positive effect of adding ZIF-8 fillers with superhydrophobic and flexible pore apertures [29]. Contrarily, $GO_{0.50}$/PIM-1 membranes showed slightly lower solvent (acetone, butanol and ethanol) uptake and higher water uptake, as expected from the

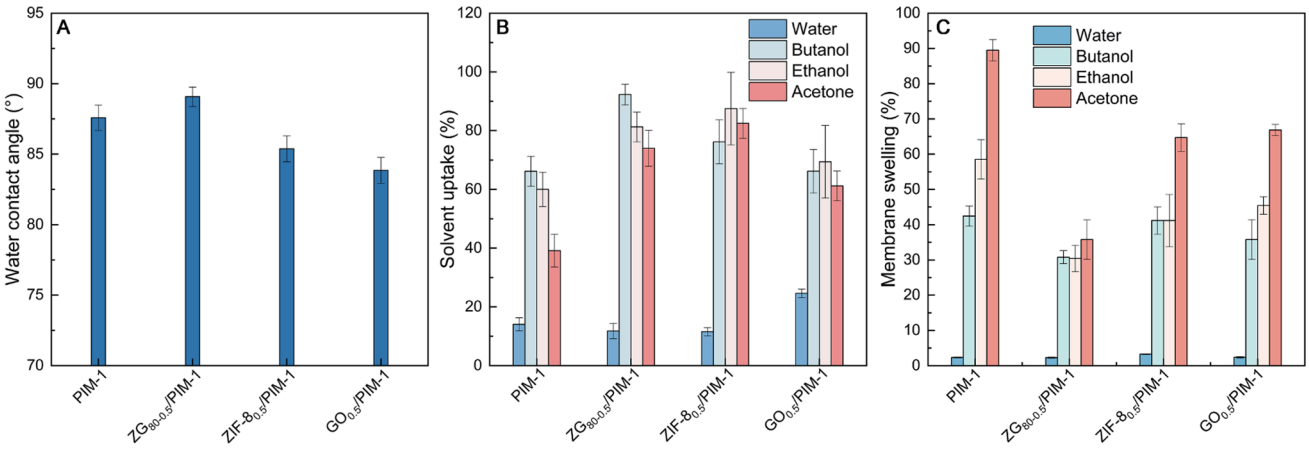

Fig. 6. Water contact angle (A), solvent uptake (B), and membrane swelling (C) of PIM-1, $ZG_{80\text{-}0.50}$/PIM-1, $ZIF\text{-}8_{0.50}$/PIM-1, and $GO_{0.50}$/PIM-1 free-standing membranes. Average measurements with standard deviations are reported; for the water contact angle, 8 measurements were carried out for each membrane, whereas 3 membrane samples were measured for solvent uptake and membrane swelling.

hydrophilic nature of the GO. Swelling was also investigated in free-standing membranes and results are summarized in the graph in Fig. 6 (C). All membranes containing fillers showed lower swelling degree than pure PIM-1 membranes when exposed to ethanol and acetone, for instance the addition of 0.5 wt% ZG_{80} led to reduced swelling values by 48.0 and 60.0%, respectively. This confirms lower mobility of PIM-1 chain fragments due to interaction with the fillers. However, the reduction in swelling was not as high for butanol, with only 27.5% for $ZG_{80\text{-}0.50}$/PIM-1 and almost no improvement for the control membranes prepared with neither non-supported ZIF-8 nor GO.

In addition, it was observed that the incorporation of ZG led to a more uniform and smoother active layer as compared to those of pristine PIM-1 thin films (SEM and AFM surface images of a range of membranes are shown in Fig. 7). The pristine PIM-1 TFC membrane (Fig. 7(A)) presented a low surface roughness of 61.0 nm. There was no statistically significant difference in the surface roughness after adding 0.25 and 0.50 wt% ZG_{80} (58.6 and 56.2 nm for $ZG_{80\text{-}0.25}$/PIM-1 and $ZG_{80\text{-}0.50}$/PIM-1, respectively) (Fig. 7(B – C)). However, when the concentration of ZG went up to 0.75 wt% the surface roughness of the TFN membrane ($ZG_{80\text{-}0.75}$/PIM-1) increased to 96.8 nm, which may be attributed to filler aggregation (Fig. 7(D)). For TFNs with GO and ZIF-8, the surface roughness was 106.8 nm and 127.4 nm, respectively (Fig. 7(E – F)), which may be ascribed to aggregation of fillers due to low dispersity of ZIF-8 and low compatibility of GO with chloroform and PIM-1. Some crystals were observed on the surface of the ZIF-8 membrane (Fig. 7(F)).

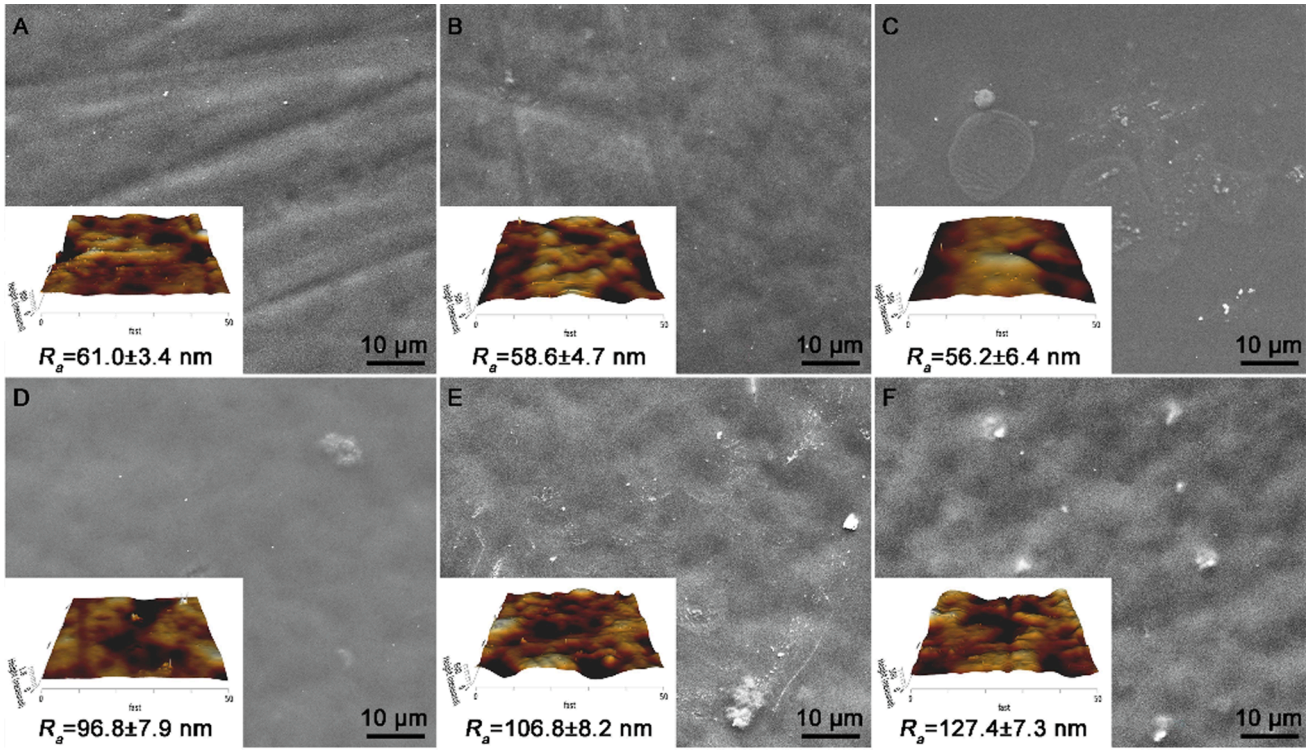

Fig. 7. SEM images of the surface of PIM-1 TFC (A) and PIM-1 TFN membranes with different fillers and loadings: $ZG_{80\text{-}0.25}$ (B), $ZG_{80\text{-}0.50}$ (C), $GZ_{80\text{-}0.75}$ (D), $GO_{0.5}$ (E), $ZIF\text{-}8_{0.5}$ (F). Insets in A–F are the AFM topography images of the membranes. Three membranes were measures to obtain the average value and standard deviation.

3.3. PV performance of ZG/PIM-1 TFN membranes

To evaluate the separation performance of the prepared membranes, PV of different aqueous solutions containing either acetone, butanol or ethanol were carried out. The performance of the PIM-1 TFC and the $ZG_{80\text{-}0.5}$/PIM-1 TFN membranes is plotted in a graph in Fig. 8. As it can be observed, the highest separation factors for both pristine PIM-1 and ZG/PIM-1 membranes are for butanol over water, in agreement with the obtained solvent uptake (Fig. 6(B)) and their lower swelling degree (Fig. 6(C)).

For the separation of butanol from water, the $ZG_{80\text{-}0.5}$/PIM-1 TFN membrane, with only 0.5 wt% of filler, showed both high flux (7.9 ± 0.69 kg $m^{-2}h^{-1}$) and the highest separation factor (29.9 ± 1.99) of all prepared membranes (the performance of TFNs with other filler loadings is discussed in Section 3.4). This results in a PV separation index (PSI) of 228 kg $m^{-2}h^{-1}$, which is among the highest values reported to date (see Fig. 9, where the performance of the TFN membranes prepared in this work is compared to the performance of other membranes found in the literature, exact values are shown in Table 1). The improvement in the membrane performance could be attributed to both, the formation of a defect-free thin active layer and the incorporation of ZG. The permeate flux of a free-standing (several tens of μm thick) $ZG_{80\text{-}0.5}$/PIM-1 membrane for butanol separation under the same testing conditions was 0.8 ± 0.08 kg $m^{-2}h^{-1}$ with a very similar separation factor to that of the TFC counterpart (30.9 ± 0.63). Compared to the freestanding and the TFC membranes of pristine PIM-1, the incorporation of ZG also improved the separation factor by 64.4 and 61.6%, respectively, with flux decreases of 13.3 and 16.8%, respectively (Fig. 9). It is also worth noting that, for a PIM-1 TFC membrane prepared without water pre-impregnation (that was reported by the group in a previous publication [11]), its separation factor (13.3) is lower than that of its free-standing counterpart (19.6 as reported in [11] and 18.8 ± 0.40 in this work), but also lower than that of the PIM-1 TFC membrane prepared with water-impregnated supports in this work (18.5 ± 1.73).

PV testing up to 40 h was conducted for the TFN membrane $ZG_{80\text{-}0.5}$/PIM-1 and the PIM-1 TFC. The performance is shown in a graph in Fig. S11; as it can be observed, the $ZG_{80\text{-}0.5}$/PIM-1 TFN showed a more stable membrane flux and separation factor than the PIM-1 TFC, which suggests certain degree of aging reduction upon the addition of the ZG. Surface and cross-sectional SEM images of the $ZG_{80\text{-}0.5}$/PIM-1 TFN membrane after the 40-h PV test are displayed in Fig. S12, where no changes to the morphology, cracks or foulants can be observed.

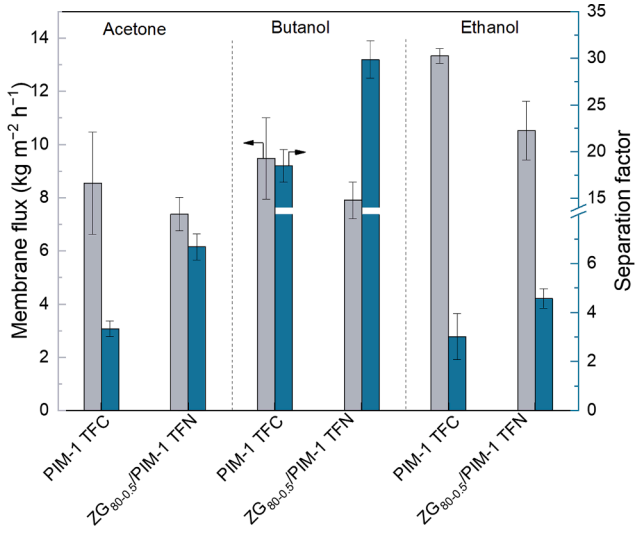

Fig. 8. PV performance of PIM-1 TFC and $ZG_{80\text{-}0.5}$/PIM-1 TFN membranes for acetone, butanol, and ethanol (Temperature = 65 °C, feed concentration = 5 wt %). Reported values are the average of 5 measurements (5 coupons for each membrane type) with standard deviations.

3.4. Unveiling the role of ZG fillers in PV

To further explore the effect of the ZG nanohybrid materials on the organophilic PV of butanol/water mixtures, PIM-1 TFN membranes with either non-supported ZIF-8 nanoparticles or GO were prepared and tested. Both the separation factor (29.9) and flux (7.9 kg $m^{-2}h^{-1}$) of the ZG-based TFN membrane $ZG_{80\text{-}0.5}$/PIM-1 were higher than those of the ZIF-8 and GO-based TFNs (Fig. 10(A)); the ZIF-$8_{0.5}$/PIM-1 membrane had a flux of 7.2 kg $m^{-2}h^{-1}$ and $\beta_{butanol/water} = 24.9$, and the $GO_{0.5}$/PIM-1 membranes had a flux of 5.4 kg $m^{-2}h^{-1}$ and $\beta_{butanol/water} = 15.5$. This is in agreement with the improved hydrophobicity, high solvent uptake, and low swelling degree of shown in the previous section for $ZG_{80\text{-}0.5}$/PIM-1 (Fig. 6), and good dispersity and compatibility with PIM-1 (Fig. 7). For all the nanocomposite membranes, the permeate flux is lower than for the purely PIM-1 TFC (9.5 kg $m^{-2}h^{-1}$). As illustrated in Fig. 10(B), all non-porous GO nanosheets, the ZG nanohybrids and the ZIF-8 nanoparticles impose a barrier effect to the feed solution, that was more pronounced for the stand-alone GO. Permeation for membranes containing ZIF-8 or ZG was still lower than that in pristine PIM-1, but higher as compared to TFNs with GO, which suggests again higher affinity between porous ZIF-8 (superhydrophobic material) and butanol and possibly solvent permeation through the ZIF-8 due to its structural flexibility. The higher $\beta_{butanol/water}$ when incorporating ZG and ZIF-8 into PIM-1 also confirms the higher affinity towards butanol is due to the presence of ZIF-8 nanoparticles. It is worth noting that the incorporation of only GO led to no improvement in the separation factor, which confirms that anti-swelling effects did not play a role in the separation (as seen for butanol in Section 3.2).

A parametric study was performed for the pervaporation of butanol/water mixtures using ZG/PIM-1 TFN membranes. Flux, $\beta_{butanol/water}$ and PSI of PIM-1 TFN membranes were plotted as a function of various parameters including the synthesis time of the GO-supported ZIF-8 (Fig. 11(A)), loading of ZG_{80} (Fig. 11(B)), and the concentration of PIM-1 in the coating solution (Fig. 11(C)). Accordingly, as the synthesis time of supported ZIF-8 extended, the loading of ZIF-8 increased, and a continuous layer of ZIF-8 was gradually formed on the GO. Therefore, both $\beta_{butanol/water}$ and flux of the resulting ZG/PIM-1 TFN membranes increased as a function of the synthesis time (Fig. 11(A)). This proves that ZIF-8 on GO can provide an efficient and selective mass transfer path for *n*-butanol. Fig. 11(B) shows that the membrane flux decreased continuously with an increase in the loading of ZG_{80} in the PIM-1. This was due to the more tortuous path for mass transfer with the presence of fillers in the membrane. Conversely, $\beta_{butanol/water}$ shows a maximum as a function of ZG loading, i.e., $\beta_{butanol/water} = 29.9$ for the membrane with 0.5 wt% ZG_{80}, suggesting that excessive loading of the filler could lead to aggregation. By comparing the PSI of the membranes, $ZG_{80\text{-}0.5}$/PIM-1 TFN membranes also gave the best performance.

Membrane flux reflects the mass transfer resistance of the active layer (PIM-1) and the substrate (PVDF). Fig. 11(C) shows that a decrease in the concentration of PIM-1 in the coating solution improved the flux of the resulting membranes. This is related to the thickness of the active layer, as shown in Fig. 5(B2), i.e. lower membrane thickness resulted in lower mass transfer resistance. Interestingly, when the concentration of PIM-1 was reduced from 2.0 to 1.0 wt%, the flux of the PIM-1 TFC membranes decreased from 9.5 to 8.2 kg $m^{-2}h^{-1}$ (Fig. S13), whilst that of the $ZG_{80\text{-}0.5}$/PIM-1 TFN membranes still showed an increase from 7.9 to 9.0 kg $m^{-2}h^{-1}$ (Fig. 11(C)). The decrease in the flux of the PIM-1 TFC membranes could be attributed to PIM-1 infiltration into the PVDF substrate and high mass transfer resistance since the interface between water and the PIM-1 solution are more likely to be disturbed as the viscosity of the coating solution decreases. The addition of the 2D ZG could help to prevent the infiltration of PIM-1 into the substrate even when the concentration of the coating solution was low.

The effect of the operating parameters including butanol

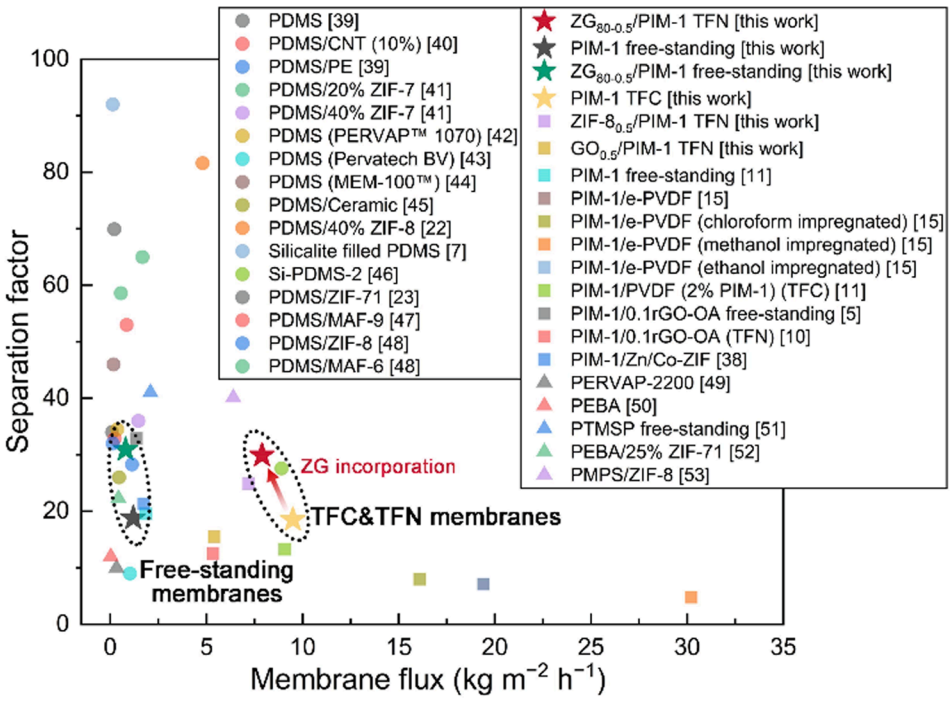

Fig. 9. Comparison of butanol/water pervaporation performance with other membranes.

Table 1
PV performance of various membranes in the separation of butanol-water mixture.

Membrane	Feed concentration (wt%)	Feed temperature (°C)	Total flux (kg $m^{-2}h^{-1}$)	β	PSI (kg $m^{-2}h^{-1}$)	Ref.
PIM-1 free-standing	5	65	1.2 ± 0.22	18.8 ± 0.40	21	This work
$ZG_{80\text{-}0.5}$/PIM-1 free-standing	5	65	0.8 ± 0.08	30.9 ± 0.63	24	This work
PIM-1 TFC	5	65	9.5 ± 1.53	18.5 ± 1.73	166	This work
$ZG_{80\text{-}0.5}$/PIM-1 TFN	5	65	7.9 ± 0.69	29.9 ± 1.99	228	This work
$ZIF\text{-}8_{0.5}$/PIM-1 TFN	5	65	7.2 ± 1.23	24.9 ± 3.94	172	This work
$GO_{0.5}$/PIM-1 TFN	5	65	5.4 ± 0.76	15.5 ± 3.31	78	This work
PIM-1 free-standing	5	65	1.85	19.6	34	[11]
PIM-1/e-PVDF	5	65	19.4 ± 0.7	7.1 ± 0.4	118	[15]
PIM-1/e-PVDF (chloroform impregnated)	5	65	16.1 ± 0.7	8 ± 0.1	113	[15]
PIM-1/e-PVDF (methanol impregnated)	5	65	30.2 ± 0.3	4.8 ± 0.1	115	[15]
PIM-1/e-PVDF (ethanol impregnated)	5	65	35.4 ± 1.8	4.8 ± 0.2	118	[15]
PIM-1/PVDF (2% PIM-1) (TFC)	5	65	9.08 ± 0.42	13.3	112	[11]
PIM-1/0.1rGO-OA free-standing	5	65	1.36	32.9 ± 10.4	43	[5]
PIM-1/0.1rGO-OA (TFN)	5	65	5.8 ± 0.6	17.0 ± 2.4	61	[10]
PIM-1/Zn/Co-ZIF	5	65	1.74	21.3		[38]
PDMS	1	37	0.095	34	3	[39]
PDMS/CNT (10%)	1.5	80	0.24	32.9	8	[40]
PDMS/PE	2	37	0.13	32	4	[39]
PDMS/20% ZIF-7	1	60	1.68	65	108	[41]
PDMS/40% ZIF-7	1	60	1.46	36	51	[41]
PDMS (PERVAP™ 1070)	<0.5	55	0.36	34.5	12	[42]
PDMS (Pervatech BV)	2	40	1.03	9	8	[43]
PDMS (MEM-100™)	2	52	0.17	46	8	[44]
PDMS/Ceramic	1	40	0.46	26	12	[45]
PDMS/40 %ZIF-8	1	80	4.8	81.6	392	[22]
Silicalite filled PDMS	1	40	9.5 ± 0.7	104 ± 1	12	[7]
Si-PDMS-2	2	80	8.9	27.6	237	[46]
PDMS/ZIF-71	2	60	0.21	69.9	15	[23]
PDMS/MAF-9	1.5	55	0.85	53	45.1	[47]
PDMS/ZIF-8	5	30	1.14	28.3	32.3	[48]
PDMS/MAF-6	5	30	0.55	58.6	32.2	[48]
PERVAP-2200	1	37	0.33	10	3.3	[49]
PEBA	1	23	0.03	12	0.3	[50]
PTMSP free-standing	6	70	2.09	41	85.7	[51]
PEBA/25% ZIF-71	1	40	0.43	22.3	9.6	[52]
PMPS/ZIF-8	1	80	6.4	40.1	250	[53]

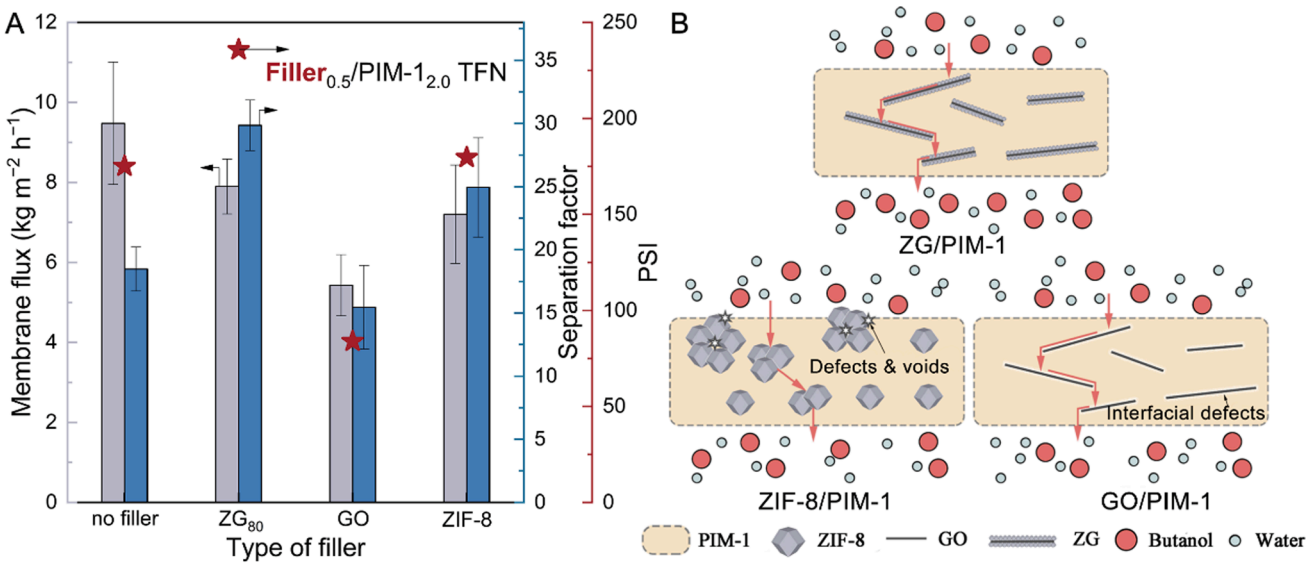

Fig. 10. Comparison of PIM-1 based membranes for butanol/water pervaporation. Temperature: 65 °C, feed concentration: 5 wt%. Red stars in A represent values of pervaporation separation index (PSI).

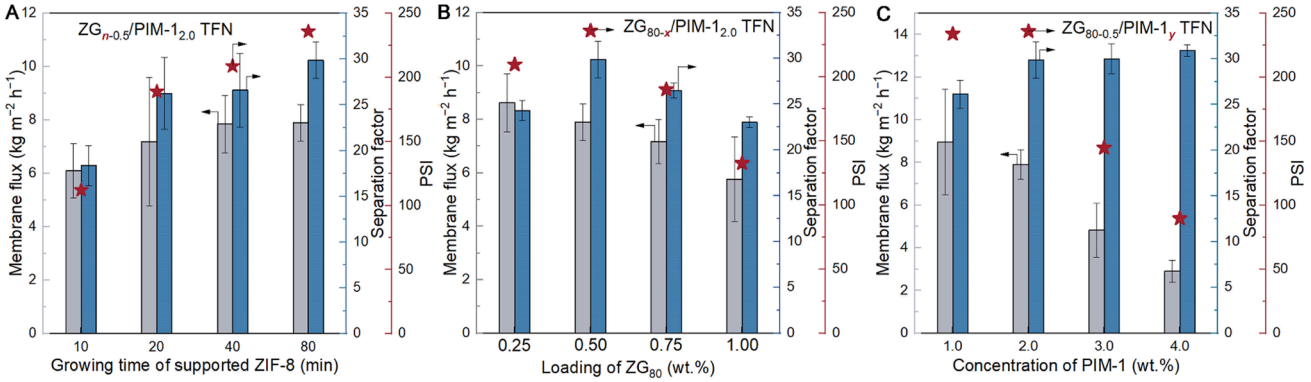

Fig. 11. Parametric study of the pervaporation performance of ZG/PIM-1 TFN membranes for butanol/water separation; A: synthesis time of ZG, B: loading of ZG_{80} and C: concentration of PIM-1 in the coating solution. The filler concentration in the TFNs in A and B is 0.5 wt%. The filler used in the TFNs in C is ZG_{80}. Red stars in the graphs are PSI values.

concentration in the feed and temperature was investigated for PIM-1 TFC and $ZG_{80\text{-}0.5}$/PIM-1 TFN membranes. Butanol flux increased with an increase in butanol concentration, whilst the water flux was relatively constant (Fig. S14 (A − B)). This is due to the increased driving force of butanol with the increased concentration in the feed; the driving force of butanol increased by ~ 4 times when butanol concentration in the feed increased from 1 to 5 wt%, the results are shown in Table S1 and were calculated using Eq. (11)–(12). Comparatively, the driving force of the water was almost constant.

In order to figure out the effect of ZG on the intrinsic property of membranes, permeability and selectivity of butanol to water of PIM-1 TFC and $ZG_{80\text{-}0.5}$/PIM-1 TFN were calculated by normalizing the driving force using Eqs. (10)–(13).The average values are shown in Fig. 12 [54]. After the addition of the ZG filler, permeabilities of both butanol and water decreased because the aforementioned increased tortuosity. However, it is worth noting that, in comparison with the PIM-1 TFC membrane, the butanol permeability decreased by 21.5%, whist the water permeability decreased by 45.3%. This could be due to the superhydrophobicity nature of the filler that prevents the adsorption and mass transfer of water. Besides, the flexible pore apertures in ZIF-8 allow the high adsorption of bio-alcohols including butanol based on the 'gate-opening' mechanism, and the continuous ZIF-8 on GO provided a selective mass transfer path for butanol [26]. Therefore, the membrane

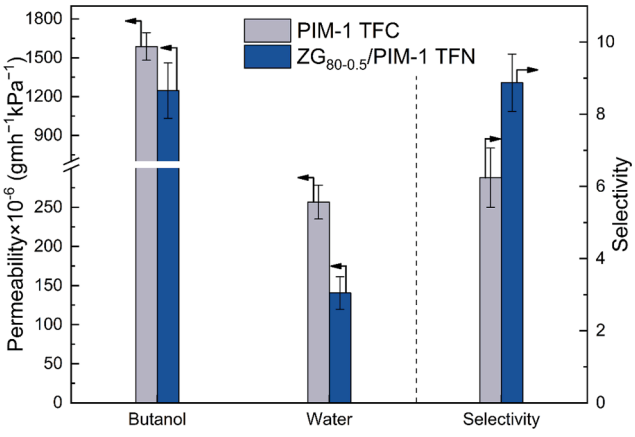

Fig. 12. Comparison of the permeability and selectivity between PIM-1 TFC and $ZG_{80\text{-}0.5}$/PIM-1 TFN.

selectivity increased from 6.2 to 8.9 with ZG as the filler. The effect of feed temperature on the pervaporation performance was also studied in the range 35–75 °C, and as expected, flux and separation factors increased (Fig. S15).

4. Conclusions

In this study, a series of PIM-1-based thin film nanocomposite membranes containing ZIF-8/GO nanohybrids were prepared via dip-coating and led to defect-free active layers (thickness < 1 μm). Polymer infiltration in the pores of the PVDF substrate did not take place due to the impregnation of the substrate with water prior to coating and the presence of 2D ZIF-8/GO (ZG) fillers in the PIM-1 coating solution. The ZG composite nanosheets were prepared by *in-situ* growth of ZIF-8 onto the surface of GO nanosheets.

The enhancement of the PV performance of the prepared TFNs was validated for butanol/water mixtures; the resulting $ZG_{80\text{-}0.5}$/PIM-1 TFN membrane showed high flux (7.9 ± 0.69 kg $m^{-2}h^{-1}$) and high separation factor (29.9 ± 1.99) that gave a PSI of 228 kg $m^{-2}h^{-1}$. This PSI value is over twice that of pure PIM-1 TFC membranes prepared without water impregnation and no fillers (PSI = 112 kg $m^{-2}h^{-1}$). The improvement is due to the formation of a defect-free active layer and synergistic effects between the ZIF-8 NPs and GO in the polymer PIM-1 matrix. The incorporation of ZG can slightly decrease the mobility of PIM-1 but it is mainly the hydrophobic nature and high affinity of ZIF-8 towards butanol that favors mass transfer of butanol over water. Furthermore, the incorporation of ZIF-8/GO can increase the free volume in the membrane and ZIF-8 nanoparticles can create preferential pathways for *n*-butanol molecules due to their high adsorption selectivity.

5. Associated content

The following files are available.

Author contributions

Boya Qiu performed experiments, data analysis, figure plotting and manuscript writing with input from all co-authors; Monica Alberto was involved in the discussion of this project and experiments & characterization, Sajjad Mohsenpour, Shengzhe Ding, Zunmin Guo, and Shaojun Xu help to conduct the characterization; Andrew Foster developed the modified synthesis of PIM-1; Peter Budd, Patricia Gorgojo, Xiaolei Fan, and Stuart Holmes took part in supervision and manuscript preparation.

CRediT authorship contribution statement

Boya Qiu: Conceptualization, Investigation, Methodology, Formal analysis, Visualization, Writing – original draft. **Monica Alberto:** Methodology. **Sajjad Mohsenpour:** Methodology. **Andrew B. Foster:** Methodology, Formal analysis, Writing – review & editing. **Shengzhe Ding:** Methodology. **Zunmin Guo:** Methodology. **Shaojun Xu:** Methodology. **Stuart M. Holmes:** Writing – review & editing. **Peter M. Budd:** Conceptualization, Writing – review & editing. **Xiaolei Fan:** Supervision, Funding acquisition, Writing – review & editing. **Patricia Gorgojo:** Conceptualization, Supervision, Project administration, Funding acquisition, Writing – review & editing.

Declaration of Competing Interest

The authors declare that they have no known competing financial interests or personal relationships that could have appeared to influence the work reported in this paper.

Data availability

Data will be made available on request.

Acknowledgements

Patricia Gorgojo is grateful to the Spanish Ministerio de Economía y Competitividad and the European Social Fund for her Ramon y Cajal Fellowship (RYC2019-027060-I/AEI/10.13039/501100011033). Boya Qiu would like to acknowledge the China Scholarship Council (CSC, file no. 202006240076)and the University of Manchester for the joint PhD studentship to support her research.

Appendix A. Supplementary material

Supplementary data to this article can be found online at https://doi.org/10.1016/j.seppur.2022.121693.

References

[1] H. Mao, H.-G. Zhen, A. Ahmad, A.-S. Zhang, Z.-P. Zhao, In situ fabrication of MOF nanoparticles in PDMS membrane via interfacial synthesis for enhanced ethanol permselective pervaporation, J. Membr. Sci. 573 (2019) 344–358.
[2] S. Fan, Z. Xiao, X. Tang, C. Chen, Y. Zhang, Q. Deng, P. Yao, W. Li, Inhibition effect of secondary metabolites accumulated in a pervaporation membrane bioreactor on ethanol fermentation of Saccharomyces cerevisiae, Bioresour. Technol. 162 (2014) 8–13.
[3] S. Fan, Z. Xiao, Y. Zhang, X. Tang, C. Chen, W. Li, Q. Deng, P. Yao, Enhanced ethanol fermentation in a pervaporation membrane bioreactor with the convenient permeate vapor recovery, Bioresour. Technol. 155 (2014) 229–234.
[4] C. Chen, L. Wang, G. Xiao, Y. Liu, Z. Xiao, Q. Deng, P. Yao, Continuous acetone–butanol–ethanol (ABE) fermentation and gas production under slight pressure in a membrane bioreactor, Bioresour. Technol. 163 (2014) 6–11.
[5] M. Alberto, J.M. Luque-Alled, L. Gao, M. Iliut, E. Prestat, L. Newman, S.J. Haigh, A. Vijayaraghavan, P.M. Budd, P. Gorgojo, Enhanced organophilic separations with mixed matrix membranes of polymers of intrinsic microporosity and graphene-like fillers, J. Membr. Sci. 526 (2017) 437–449.
[6] H. Zhou, J. Zhang, Y. Wan, W. Jin, Fabrication of high silicalite-1 content filled PDMS thin composite pervaporation membrane for the separation of ethanol from aqueous solutions, J. Membr. Sci. 524 (2017) 1–11.
[7] S. Claes, P. Vandezande, S. Mullens, K. De Sitter, R. Peeters, M.K. Van Bael, Preparation and benchmarking of thin film supported PTMSP-silica pervaporation membranes, J. Membr. Sci. 389 (2012) 265–271.
[8] E.A. Fouad, X. Feng, Use of pervaporation to separate butanol from dilute aqueous solutions: Effects of operating conditions and concentration polarization, J. Membr. Sci. 323 (2) (2008) 428–435.
[9] H. Tan, Y. Wu, T. Li, Pervaporation of n-butanol aqueous solution through ZSM-5-PEBA composite membranes, J. Appl. Polym. Sci. 129 (1) (2013) 105–112.
[10] M. Alberto, R. Bhavsar, J.M. Luque-Alled, E. Prestat, L. Gao, P.M. Budd, A. Vijayaraghavan, G. Szekely, S.M. Holmes, P. Gorgojo, Study on the formation of thin film nanocomposite (TFN) membranes of polymers of intrinsic microporosity and graphene-like fillers: Effect of lateral flake size and chemical functionalization, J. Membr. Sci. 565 (2018) 390–401.
[11] L. Gao, M. Alberto, P. Gorgojo, G. Szekely, P.M. Budd, High-flux PIM-1/PVDF thin film composite membranes for 1-butanol/water pervaporation, J. Membr. Sci. 529 (2017) 207–214.
[12] E.A. Baroncini, S. Kumar Yadav, G.R. Palmese, J.F. Stanzione, Recent advances in bio-based epoxy resins and bio-based epoxy curing agents, J. Appl. Polym. Sci. 133 (45) (2016).
[13] P. Gorgojo, S. Karan, H.C. Wong, M.F. Jimenez-Solomon, J.T. Cabral, A. G. Livingston, Ultrathin Polymer Films with Intrinsic Microporosity: Anomalous Solvent Permeation and High Flux Membranes, Adv. Funct. Mater. 24 (30) (2014) 4729–4737.
[14] J. Li, M. Zhang, W. Feng, L. Zhu, L. Zhang, PIM-1 pore-filled thin film composite membranes for tunable organic solvent nanofiltration, J. Membr. Sci. 601 (2020), 117951.
[15] J. Contreras-Martínez, S. Mohsenpour, A.W. Ameen, P.M. Budd, C. García-Payo, M. Khayet, P. Gorgojo, High-Flux Thin Film Composite PIM-1 Membranes for Butanol Recovery: Experimental Study and Process Simulations, ACS Appl. Mater. Interfaces 13 (36) (2021) 42635–42649.
[16] H. Zeng, S. He, S.S. Hosseini, B. Zhu, L. Shao, Emerging nanomaterial incorporated membranes for gas separation and pervaporation towards energetic-efficient applications, Adv. Membr. 2 (2022), 100015.
[17] J. Yao, H. Wang, Zeolitic imidazolate framework composite membranes and thin films: synthesis and applications, Chem. Soc. Rev. 43 (13) (2014) 4470–4493.
[18] S. Yuan, X. Li, J. Zhu, G. Zhang, P. Van Puyvelde, B. Van der Bruggen, Covalent organic frameworks for membrane separation, Chem. Soc. Rev. 48 (10) (2019) 2665–2681.

[19] A.F. Ismail, P.S. Goh, S.M. Sanip, M. Aziz, Transport and separation properties of carbon nanotube-mixed matrix membrane, Sep. Purif. Technol. 70 (1) (2009) 12–26.
[20] S. Mohsenpour, A.W. Ameen, S. Leaper, C. Skuse, F. Almansour, P.M. Budd, P. Gorgojo, PIM-1 Membranes Containing POSS - Graphene Oxide for CO2 Separation, Sep. Purif. Technol. 298 (2022) 121447.
[21] S. Li, Z. Chen, Y. Yang, Z. Si, P. Li, P. Qin, T. Tan, Improving the pervaporation performance of PDMS membranes for n-butanol by incorporating silane-modified ZIF-8 particles, Sep. Purif. Technol. 215 (2019) 163–172.
[22] H. Fan, Q.i. Shi, H. Yan, S. Ji, J. Dong, G. Zhang, Simultaneous Spray Self-Assembly of Highly Loaded ZIF-8–PDMS Nanohybrid Membranes Exhibiting Exceptionally High Biobutanol-Permselective Pervaporation, Angew. Chem. Int. Ed. 53 (22) (2014) 5578–5582.
[23] H. Yin, C.Y. Lau, M. Rozowski, C. Howard, Y. Xu, T. Lai, M.E. Dose, R.P. Lively, M. L. Lind, Free-standing ZIF-71/PDMS nanocomposite membranes for the recovery of ethanol and 1-butanol from water through pervaporation, J. Membr. Sci. 529 (2017) 286–292.
[24] H. Yin, A. Khosravi, L. O'Connor, A.Q. Tagaban, L. Wilson, B. Houck, Q. Liu, M. L. Lind, Effect of ZIF-71 Particle Size on Free-Standing ZIF-71/PDMS Composite Membrane Performances for Ethanol and 1-Butanol Removal from Water through Pervaporation, Ind. Eng. Chem. Res. 56 (32) (2017) 9167–9176.
[25] G. Zhang, J. Li, N. Wang, H. Fan, R. Zhang, G. Zhang, S. Ji, Enhanced flux of polydimethylsiloxane membrane for ethanol permselective pervaporation via incorporation of MIL-53 particles, J. Membr. Sci. 492 (2015) 322–330.
[26] H. Fan, Q.i. Shi, H. Yan, S. Ji, J. Dong, G. Zhang, Simultaneous spray self-assembly of highly loaded ZIF-8-PDMS nanohybrid membranes exhibiting exceptionally high biobutanol-permselective pervaporation, Angewandte Chemie – Int. Ed. 53 (22) (2014) 5578–5582.
[27] M. Liu, M.D. Nothling, P.A. Webley, J. Jin, Q. Fu, G.G. Qiao, High-throughput CO2 capture using PIM-1@MOF based thin film composite membranes, Chem. Eng. J. 396 (2020), 125328.
[28] E. Aliyev, J. Warfsmann, B. Tokay, S. Shishatskiy, Y.-J. Lee, J. Lillepaerg, N. R. Champness, V. Filiz, Gas Transport Properties of the Metal-Organic Framework (MOF)-Assisted Polymer of Intrinsic Microporosity (PIM-1) Thin-Film Composite Membranes, ACS Sustain. Chem. Eng. 9 (2) (2021) 684–694.
[29] R. Hu, G. Zhao, Y. He, H. Zhu, The application feasibility of graphene oxide membranes for pressure-driven desalination in a dead-end flow system, Desalination 477 (2020), 114271.
[30] W. Li, J. Li, N. Wang, X. Li, Y. Zhang, Q. Ye, S. Ji, Q.-F. An, Recovery of bio-butanol from aqueous solution with ZIF-8 modified graphene oxide composite membrane, J. Membr. Sci. 598 (2020), 117671.
[31] Y. Hu, J. Wei, Y. Liang, H. Zhang, X. Zhang, W. Shen, H. Wang, Zeolitic Imidazolate Framework/Graphene Oxide Hybrid Nanosheets as Seeds for the Growth of Ultrathin Molecular Sieving Membranes, Angew. Chem. Int. Ed. 55 (6) (2016) 2048–2052.
[32] A.B. Foster, M. Tamaddondar, J.M. Luque-Alled, W.J. Harrison, Z.e. Li, P. Gorgojo, P.M. Budd, Understanding the Topology of the Polymer of Intrinsic Microporosity PIM-1: Cyclics, Tadpoles, and Network Structures and Their Impact on Membrane Performance, Macromolecules 53 (2) (2020) 569–583.
[33] S.R. Venna, M.A. Carreon, Highly Permeable Zeolite Imidazolate Framework-8 Membranes for CO2/CH4 Separation, J. Am. Chem. Soc. 132 (1) (2010) 76–78.
[34] S.R. Venna, J.B. Jasinski, M.A. Carreon, Structural Evolution of Zeolitic Imidazolate Framework-8, J. Am. Chem. Soc. 132 (51) (2010) 18030–18033.
[35] H.B. Park, J. Kamcev, L.M. Robeson, M. Elimelech, B.D. Freeman, Maximizing the right stuff: The trade-off between membrane permeability and selectivity, Science 356(6343) (2017) p. eaab0530.
[36] T. Rodenas, I. Luz, G. Prieto, B. Seoane, H. Miro, A. Corma, F. Kapteijn, F.X. Llabrés i Xamena, J. Gascon, Metal–organic framework nanosheets in polymer composite materials for gas separation, Nat. Mater. 14 (1) (2015) 48–55.
[37] B. Qiu, S. Fan, Y.u. Chen, J. Chen, Y. Wang, Y. Wang, J. Liu, Z. Xiao, Micromembrane absorber with deep-permeation nanostructure assembled by flowing synthesis, AIChE J. 67 (8) (2021).
[38] T.H. Butt, R. Tamime, P.M. Budd, W.J. Harrison, Z. Shamair, A. Laeeq Khan, Enhancing the organophilic separations with mixed matrix membranes of PIM-1 and bimetallic Zn/Co-ZIF filler, Sep. Purif. Technol. 283 (2022), 120216.
[39] S.-Y. Li, R. Srivastava, R.S. Parnas, Separation of 1-butanol by pervaporation using a novel tri-layer PDMS composite membrane, J. Membr. Sci. 363 (1) (2010) 287–294.
[40] C. Xue, G.-Q. Du, L.-J. Chen, J.-G. Ren, J.-X. Sun, F.-W. Bai, S.-T. Yang, A carbon nanotube filled polydimethylsiloxane hybrid membrane for enhanced butanol recovery, Sci. Rep. 4 (2014) 5925.
[41] X. Wang, J. Chen, M. Fang, T. Wang, L. Yu, J. Li, ZIF-7/PDMS mixed matrix membranes for pervaporation recovery of butanol from aqueous solution, Sep. Purif. Technol. 163 (2016) 39–47.
[42] E.A. Fouad, X. Feng, Pervaporative separation of n-butanol from dilute aqueous solutions using silicalite-filled poly(dimethyl siloxane) membranes, J. Membr. Sci. 339 (1) (2009) 120–125.
[43] S. Van Wyk, A. Van der Ham, S. Kersten, Pervaporative separation and intensification of downstream recovery of acetone-butanol-ethanol (ABE), Chem. Eng. Process.-Process Intensification 130 (2018) 148–159.
[44] A.G. Fadeev, M.M. Meagher, S.S. Kelley, V.V. Volkov, Fouling of poly [-1-(trimethylsilyl)-1-propyne] membranes in pervaporative recovery of butanol from aqueous solutions and ABE fermentation broth, J. Membr. Sci. 173 (1) (2000) 133–144.
[45] G. Liu, D. Hou, W. Wei, F. Xiangli, W. Jin, Pervaporation Separation of Butanol-Water Mixtures Using Polydimethylsiloxane/Ceramic Composite Membrane, Chin. J. Chem. Eng. 19 (1) (2011) 40–44.
[46] X. Liu, Y. Li, Y.i. Liu, G. Zhu, J. Liu, W. Yang, Capillary supported ultrathin homogeneous silicalite-poly(dimethylsiloxane) nanocomposite membrane for bio-butanol recovery, J. Membr. Sci. 369 (1-2) (2011) 228–232.
[47] C. Ren, Z. Si, Y. Qu, S. Li, H. Wu, F. Meng, X. Zhang, Y. Wang, C. Liu, P. Qin, CF3-MOF enhanced pervaporation selectivity of PDMS membranes for butanol separation, Sep. Purif. Technol. 284 (2022), 120255.
[48] G. Wu, Q. Fan, W. Sun, Z. Yu, Z. Jia, J. Ma, Regulatable pervaporation performance of Zn-MOFs/polydimethylsiloxane mixed matrix pervaporation membranes, Chin. J. Chem. Eng. 42 (2022) 312–318.
[49] E. El-Zanati, E. Abdel-Hakim, O. El-Ardi, M. Fahmy, Modeling and simulation of butanol separation from aqueous solutions using pervaporation, J. Membr. Sci. 280 (1-2) (2006) 278–283.
[50] F. Liu, L. Liu, X. Feng, Separation of acetone–butanol–ethanol (ABE) from dilute aqueous solutions by pervaporation, Sep. Purif. Technol. 42 (3) (2005) 273–282.
[51] A.G. Fadeev, Y.A. Selinskaya, S.S. Kelley, M.M. Meagher, E.G. Litvinova, V. S. Khotimsky, V.V. Volkov, Extraction of butanol from aqueous solutions by pervaporation through poly(1-trimethylsilyl-1-propyne), J. Membr. Sci. 186 (2) (2001) 205–217.
[52] S. Liu, G. Liu, X. Zhao, W. Jin, Hydrophobic-ZIF-71 filled PEBA mixed matrix membranes for recovery of biobutanol via pervaporation, J. Membr. Sci. 446 (2013) 181–188.
[53] X.-L. Liu, Y.-S. Li, G.-Q. Zhu, Y.-J. Ban, L.-Y. Xu, W.-S. Yang, An Organophilic Pervaporation Membrane Derived from Metal-Organic Framework Nanoparticles for Efficient Recovery of Bio-Alcohols, Angew. Chem. Int. Ed. 50 (45) (2011) 10636–10639.
[54] R.W. Baker, J.G. Wijmans, Y. Huang, Permeability, permeance and selectivity: A preferred way of reporting pervaporation performance data, J. Membr. Sci. 348 (1) (2010) 346–352.